PNAS RESEARCH ARTICLE | DEVELOPMENTAL BIOLOGY OPEN ACCESS

Ret deficiency decreases neural crest progenitor proliferation and restricts fate potential during enteric nervous system development

Elizabeth Vincent[a,1], Sumantra Chatterjee[b,c,1], Gabrielle H. Cannon[a], Dallas Auer[a], Holly Ross[a], Aravinda Chakravarti[b,c,2], and Loyal A. Goff[a,d,e,2]

Contributed by Aravinda Chakravarti; received July 14, 2022; accepted July 18, 2023; reviewed by Tiffany A. Heanue and Ramnik J. Xavier

The receptor tyrosine kinase RET plays a critical role in the fate specification of enteric neural crest–derived cells (ENCDCs) during enteric nervous system (ENS) development. *RET* loss of function (LoF) is associated with Hirschsprung disease (HSCR), which is marked by aganglionosis of the gastrointestinal (GI) tract. Although the major phenotypic consequences and the underlying transcriptional changes from *Ret* LoF in the developing ENS have been described, cell type- and state-specific effects are unknown. We performed single-cell RNA sequencing on an enriched population of ENCDCs from the developing GI tract of *Ret* null heterozygous and homozygous mice at embryonic day (E)12.5 and E14.5. We demonstrate four significant findings: 1) *Ret*-expressing ENCDCs are a heterogeneous population comprising ENS progenitors as well as glial- and neuronal-committed cells; 2) neurons committed to a predominantly inhibitory motor neuron developmental trajectory are not produced under *Ret* LoF, leaving behind a mostly excitatory motor neuron developmental program; 3) expression patterns of HSCR-associated and *Ret* gene regulatory network genes are impacted by *Ret* LoF; and 4) *Ret* deficiency leads to precocious differentiation and reduction in the number of proliferating ENS precursors. Our results support a model in which *Ret* contributes to multiple distinct cellular phenotypes during development of the ENS, including the specification of inhibitory neuron subtypes, cell cycle dynamics of ENS progenitors, and the developmental timing of neuronal and glial commitment.

enteric nervous system | single-cell RNA-seq | *Ret* | Hirschsprung disease | cell cycle dysregulation

Significance

Hirschsprung disease (HSCR) is a developmental disorder arising from the inability of enteric neural crest–derived cells (ENCDCs) to properly proliferate and migrate to form a functional enteric nervous system (ENS). Approximately 50% of HSCR patients harbor LoF variants at the receptor tyrosine kinase gene *RET*. To decipher the cell type–specific effects underlying *Ret* LoF, we examined the cellular heterogeneity of the ENS during mouse gastrointestinal tract development in the presence and absence of *Ret*, using single-cell RNA sequencing. Consistent with prior observations, we demonstrate that *Ret* deficiency leads to precocious differentiation and reduction in the number of proliferating ENS precursors. Our analysis further demonstrates that *Ret* expression is required for neuronal commitment to a specific postmitotic developmental trajectory.

The ENS is derived from migrating vagal and sacral neural crest cells (1–5) that colonize the developing gut between embryonic day (E)9.5 to E14.5 in mice (6) and Carnegie stage (CS) 14 to CS22 in humans (7), leading to the neuronal networks of the myenteric and submucosal plexuses. Beyond the neural crest origins of ENS, lineage tracing studies have demonstrated that a small portion of both neuronal and glial cells in the ENS are also derived from Schwann cell precursors (SCPs) (8).

The ENS has multiple essential roles in motility, absorption, and immunity (9), and disruption of proper ENS development or organization underlies several disorders of the gastrointestinal system (10). Previous studies of ENS development have demonstrated that invading enteric neural crest–derived cells (ENCDCs) are predominantly neuronal precursors early in mouse development (E10.5), but as development proceeds, they differentiate into either glia, expressing classical glial markers including *Gfap, Plp1,* and *S100b* (11, 12), or neurons (11). Single-cell transcriptional profiling of mouse ENCDCs during mid and late (E12.5, E15.5, and E18.5) developmental time points reflects this heterogeneity and temporal change in cell fate (13–16).

One of the key factors involved in the migration and differentiation of ENCDCs into the developing gut is the receptor tyrosine kinase RET (13, 17). RET expression in ENCDCs promotes proliferation and cell survival via the MAPK and PI3K/AKT pathways (18). *RET* LoF leads to HSCR, an uncommon (~1/5,000 live births) developmental disorder of the ENS characterized by the absence of enteric ganglia along variable lengths of the distal bowel (19–23). In the developing mouse gut, *Ret* deficiency leads to significant transcriptional changes in transcription factors, signaling molecules, and genes involved in specific transport and biosynthesis processes, leading to aganglionosis (24, 25). Tissue-level bulk transcriptomic studies in *Ret*-deficient developing mouse gut (24, 25) have uncovered significant expression changes in genes harboring mutations in HSCR patients such as *Ednrb*,*Gdnf, Sox10, Pax3, and Phox2b* (24–28).

Development and fate specification in the ENS occurs in conjunction with migration along the forming gut tube (12, 29). As such, temporal and spatial influences affect ENCDC competence and can modulate fate decisions during development (12, 30). While *Ret* is known to play a role in the proper establishment of the ENS, the cell

Author contributions: E.V., S.C., A.C., and L.A.G. designed research; E.V., S.C., G.H.C., D.A., and H.R. performed research; L.A.G. contributed new reagents/analytic tools; E.V., S.C., A.C., and L.A.G. analyzed data; and E.V., S.C., A.C., and L.A.G. wrote the paper.

Reviewers: T.A.H., The Francis Crick Institute; and R.J.X., Broad Institute.

The authors declare no competing interest.

[1]E.V. and S.C. contributed equally to this work.

[2]To whom correspondence may be addressed. Email: aravinda.chakravarti@nyulangone.org or loyalgoff@jhmi.edu.

This article contains supporting information online at https://www.pnas.org/lookup/suppl/doi:10.1073/pnas.2211986120/-/DCSupplemental.

Published August 16, 2023.

type–specific effects of *Ret* LoF on normal ENS development have not yet been elucidated and could contribute to our understanding of normal ENS development.

To identify the cell type–specific contributions of *Ret* to the proper organization and development of the ENS, we examined the cellular heterogeneity of the ENS during mouse gut development in the presence and absence of *Ret*. We profiled the transcriptomes of 1,003 *Ret*-expressing single cells in heterozygous and homozygous *Ret*-null mice at E12.5 and E14.5. *Ret* heterozygous mice do not exhibit aganglionosis in the developing gut or any other known phenotypes associated with *Ret* LOF and hence serve as a suitable control for our study. ENCDCs and their progeny were isolated using a cyan fluorescent protein (CFP) reporter driven by the endogenous *Ret* promoter for enrichment (31). Using a combination of differential gene expression analysis, gene coexpression pattern analysis, RNA velocity, and cell cycle state predictions, we identify several key developmental phenotypes associated with loss of *Ret.* The specific effects of *Ret* LoF vary across different cellular states in ENCDCs, including effects on progenitor proliferation, migration, differentiation, and fate specification. We confirm a previously described bifurcation in enteric neuronal developmental fate specification (14, 16) at an earlier time point. We further demonstrate that *Ret* expression is required for commitment to one of these two neuronal fates and, subsequently, the establishment of cell types from a predominantly inhibitory neuron developmental trajectory. Additionally, we show that homozygous *Ret* LoF leads to precocious differentiation of ENCDCs and a reduction in ENCDC progenitor proliferation rate. Each of these observed phenotypes may independently contribute to the deficits in proper ENS development, organization, and function observed in HSCR. These results highlight the diverse cell type–specific roles for *Ret* in the proper development of the ENS, with implications for understanding HSCR-related phenotypes.

Results

To assess cell type–specific roles for *Ret* in the developing ENS, we used a previously described mouse line harboring a *Ret*-null fluorescent reporter allele (Ret^{CFP}) (31). All ENCDCs express *Ret* during early development (17), enabling isolation via FACS in this reporter system. *Ret*-null ($Ret^{CFP/CFP}$) mouse embryos exhibit total colonic aganglionosis and kidney agenesis and are perinatal lethal (31). Importantly, no defects in ENS formation have been observed in *Ret*-heterozygous ($Ret^{CFP/+}$) mice (31), nor any significant difference in genome-wide expression compared to wild-type (WT) GI tract (32). Comparison of $Ret^{CFP/CFP}$ to $Ret^{CFP/+}$ mice can therefore elucidate the mechanisms by which *Ret* LoF affects the proper formation of the ENS.

To investigate transcriptional changes of ENCDCs, we performed single-cell RNA sequencing (scRNA-seq) on FACS-enriched populations of ENCDCs in the developing murine gut. Briefly, CFP-positive single cells were collected from dissociated stomach and intestine of male and female embryos from $Ret^{CFP/+}$ *and* $Ret^{CFP/CFP}$ at E12.5 and E14.5, and subjected to a modified Smart-seq2 scRNA-Seq library preparation (33, 34) (*Methods*). Libraries from 95 cells for each of two biological replicates were sequenced from all age, sex, and genotype combinations, with the exception of E14.5 $Ret^{CFP/CFP}$ embryos. Consistent with a previously described reduction in CFP^+ cells in a *Ret* hypomorphic mouse model (31), we observed reduction in the cell capture rate in the E14.5 $Ret^{CFP/CFP}$ mice as compared to other ages and genotypes. We also observed a pronounced sex bias in the number of CFP^+ cells recovered from E14.5 $Ret^{CFP/CFP}$ embryos, with fewer viable cells collected from males, consistent with the established sex bias observed in HSCR (35) and described in other mouse models of HSCR (31, 36). As such, only 22 cells from one male E14.5 $Ret^{CFP/CFP}$ embryo and 190 cells from four female E14.5 $Ret^{CFP/CFP}$ embryos were recovered (Dataset S1). Full-length cDNA scRNA-Seq libraries from 1,341 individual cells were sequenced to an average depth of 9.91×10^5 (SD 7.43×10^5) paired-end reads per cell. Low-quality cells were removed using standard metrics (*Methods*) leaving 1,003 cells (Fig. 1*A* and Dataset S1) with an average read depth of 1.16×10^6 (SD 6.83×10^5) paired-end reads per cell. Relative FPKM values were converted to estimated RNA copies per cell (CPC) using the CENSUS algorithm (37). We identified a set of 14,319 expressed genes with greater than zero CPC in at least 20 cells and a SD greater than zero across all cells. To visualize the transcriptional relationships between cells, we identified a set of 419 high-variance genes (*Methods*) to use as input for uniform manifold approximation and projection (UMAP) dimensionality reduction to establish a biologically relevant, two-dimensional embedding of the cells (Fig. 1*B* and *SI Appendix*, Fig. S1).

Annotation of Cell Types and States of the Developing ENS. To quantify cell type and cell state differences with respect to genotype, we first used a Gaussian-based clustering algorithm (38) to identify nine clusters (Fig. 1*C*) and calculated gene-wise specificity scores to identify gene expression profiles for each cluster (*SI Appendix*, Fig. S2*A*). High specificity scores relative to mean expression identified clusters of actively cycling progenitors (cluster 2, *Hist1h* family genes; cluster 3, *Aurka/b* and *Cdk1*), a neurogenic commitment window (cluster 4, *Neurod4*; cluster 5, *Pcp2* and *Hes5*; cluster 6, *Hes6* and *Btg2*) (39, 40), maturing neurons (cluster 7, *Etv1*, *Vip*, *Gal,* and *Cartpt*; cluster 8, *Slc18a3 (VAChT), Npy, Snap25,* and *Gfra2*; cluster 9, *Th, Dbh,* and *Ddc*) (41–43), and a population of postmitotic glial-committed cells (cluster 1, *Plp1* and *Myl9*) (44) (*SI Appendix*, Fig. S2*B* and Dataset S2). The neural progenitor cell marker p75 (*Ngfr*) and the pan-neuronal marker TuJ1 (*Tubb3*), used to label mature enteric neurons along with *Ret* (11, 45), have distinct, largely nonoverlapping expression profiles in *Ret*-expressing cells at these time points (*SI Appendix*, Fig. S2*C*).

To annotate cells as either progenitors, developing glia, or developing neurons, we evaluated canonical marker gene expression for mature ENS cell types. However, during development, the majority of cells may not yet express markers of mature, terminally differentiated cell types. To address this, we assigned cell types using a combination of transfer learning and marker gene expression to predict the most likely annotation based on an existing cellular atlas of adult mouse enteric neurons and glia (46). To uncover transcriptional signatures of mature ENS cell types, we learned patterns of gene coexpression on the annotated set of enteric neurons and glia from the public dataset using single-cell Coordinated Gene Activity in Pattern Sets (scCoGAPS) (47) and trained a random forest (RF) model on those learned patterns to predict cell type (*Methods*). We next projected our single-cell data into the latent spaces defined by these patterns using projectR (47, 48) (*SI Appendix*, Fig. S3) and employed the RF model to classify cells based on their projected pattern weights (*SI Appendix*, Fig. S4 *A–C*). We next calculated cell type proportions by cluster (*SI Appendix*, Fig. S4*D*). For clusters in which at least 90% of cells shared an annotation, we transferred the majority annotation to all members of the cluster. As a result, clusters 1 to 5 (1 = 99% glia, 2 = 98%, 3 = 92%, 4 = 95%, and 5 = 94%) were annotated as glia, and clusters 7 and 8 (7 = 98% neuron and 8 = 90%) were annotated as neurons. Annotations for clusters 6 (58% glia) and 9 (63% neuron) were not altered.

Our single-cell gene expression profiling is a snapshot in development for cells that have not yet committed to mature identities.

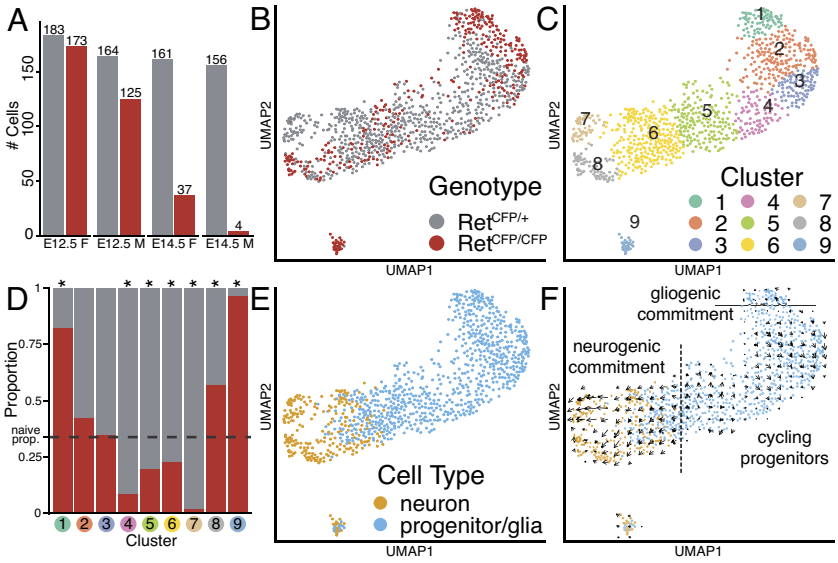

Fig. 1. A cellular map of *Ret*-expressing enteric nervous system cells. (*A*) Bar plot of post-quality-control count of sorted $Ret^{CFP/+}$ and $Ret^{CFP/CFP}$ expressing cells from E12.5 and E14.5 embryonic gut in male and female mice. (*B* and *C*) UMAP of 1,003 cells colored by (*B*) genotype and (*C*) cluster. (*D*) Stacked bar plot of genotype proportions by cluster. Asterisk denotes SD from naive proportion (chi-squared test for equal proportions, corrected $P < 0.05$). (*E* and *F*) UMAP colored by predicted cell type (*F*) with RNA velocity vector field superimposed. The dotted line indicates neurogenic commitment, and the solid line indicates gliogenic commitment.

To infer the direction of state transitions for our ENCDC population, we calculated RNA velocity estimates (49) and observed that the velocity field models diverging trajectories from a common origin (Fig. 1*F*). Cells with high projection weights in patterns associated with proliferating ENCDCs (pattern 40: *Brca1/2*, *Cdc6*, and *Pola1/2*; pattern 41: *Ccna1/b1*, *Cenpe*, and *Kif24*; pattern 42: *Aurka/b*, *Bub1*, and *Top2a*; *SI Appendix*, Fig. S3 and Datasets S3–S5) (50, 51) exhibit an ellipsoid pattern of velocities, consistent with transition through the cell cycle. Extending from this progenitor population, we observed a cluster of cells expressing canonical markers consistent with progression toward a neuronal fate (cluster 6: *Btg2* and *Hes6*, *SI Appendix*, Fig. S2*B*) (39, 40) that further branches into two distinct trajectories of neuronal specification (Fig. 1*F*), consistent with previous observations of postmitotic branching of cellular fate specification for neural crest–derived neurons in later gut development (14). We infer through shared marker gene expression that cluster 7 in our data corresponds to developmental branch (branch A) ($Etv1^+$, $Nos1^+$, Vip^+, and Gal^+), and cluster 8 corresponds to developmental branch B ($Bnc2^+$, $Dlx5^+$, $Mgat4c^+$, and $Ndufa4l2^+$) (*SI Appendix*, Fig. S6*A*), as described previously in E15.5-E18.5 small intestine from WT mice (14). These data highlight that *Ret*-expressing cells isolated from the GI tract encompass two broad fates during development (glial or neuronal commitment) and confirm that neuronally committed ENCDCs diverge postmitotically into two distinct developmental trajectories, outlining the diversity of cellular fate trajectories accessible to ENCDCs within the developing mouse gut.

***Ret* LoF Induces Distinct Transcriptional Responses in Different ENS Cell States.** We asked whether loss of *Ret* changes the proportion of ENCDC subtypes in our dataset. To assess this, we tested for genotype bias in cluster composition by comparing the proportion of $Ret^{CFP/CFP}$ cells against the naive (overall) proportion of 34%. Using a chi-squared test for equal proportions, we observed significant deviations in seven of the nine identified clusters: clusters 1, 8, and 9 are enriched for $Ret^{CFP/CFP}$ cells (cluster 1: 83%, Bonferroni-adjusted $P = 9.86 \times 10^{-18}$; cluster 8: 57%, $P = 5.64 \times 10^{-4}$; cluster 9: 97%, $P = 1.24 \times 10^{-11}$), clusters 4 to 7 are depleted for $Ret^{CFP/CFP}$ cells (cluster 4: 9%, Bonferroni-adjusted $P = 3.48 \times 10^{-5}$; cluster 5: 20%, $P = 1.00 \times 10^{-3}$; cluster 6: 33%, $P = 3.44 \times 10^{-3}$; cluster 7: 2%, $P = 6.33 \times 10^{-5}$), while clusters 2 and 3 are relatively invariant (cluster 2: 42% $Ret^{CFP/CFP}$, Bonferroni-adjusted $P = 0.196$; cluster 3: 35%, $P = 1.0$) (Fig. 1*D*). Clusters 6, 7, and 8 are neuronal-committed clusters and differ significantly from the naive proportion. Clusters 6 and 7 are enriched for $Ret^{CFP/+}$ cells and 8 is enriched for $Ret^{CFP/CFP}$ cells, indicating strong genotypic effects associated with neuronal fate specification. Three glial clusters (1, 4, and 5) differ significantly from the naive proportion as well, with cluster 1 enriched for and clusters 4 and 5 depleted of $Ret^{CFP/CFP}$ cells. Cluster-specific enrichment of genotype within the neuronal and glial populations suggests that genotypic effects of *Ret* LoF modulate cell fate commitment with divergent results across ENCDC cell states.

Consistent with previous studies (8, 52, 53), the majority of *Ret*-null cells captured in our assay correspond to cells associated with vagal nerve fibers in the proximal stomach and are therefore parasympatho-enteric neural crest–derived, and hence derived from SCPs (Fig. 2*E*). The only cluster separate from the primary manifold is cluster 9, which is enriched for $Ret^{CFP/CFP}$ cells (29/30, 97%, $P = 1.24 \times 10^{-11}$, Fig. 1*D*). This cluster represents a transcriptionally distinct population that expresses markers of sacrally derived SCPs (*Th+, Dbh+)* as well as differential Hox gene expression consistent with more caudal development. Specifically, cluster 9 cells exhibit decreased expression of rostral Hox genes and increased expression of caudal Hox genes (*SI Appendix*, Fig. S5), indicating that these cells may derive from the CFP+ cells detected in the distal hindgut at E14.5 (Fig. 2*E*). This population likely corresponds to sacral neural crest cells that colonize the hindgut in a caudorostral direction around E14.5 (29, 54–56). While cluster 9 is enriched for $Ret^{CFP/CFP}$ cells, the majority of cells in cluster 9 (28/30) derive from only one of the nine $Ret^{CFP/CFP}$ embryos sampled, thereby limiting our ability to make definitive interpretations with respect to genotype.

To identify the transcriptional effects of *Ret* LoF on the developing ENS, we tested 14,319 genes and identified 520 as differentially expressed (DE) with respect to genotype across all cells (monocle likelihood ratio test; Benjamini–Hochberg corrected q value < 0.05, Fig. 2*A* and Dataset S6A). Hierarchical clustering

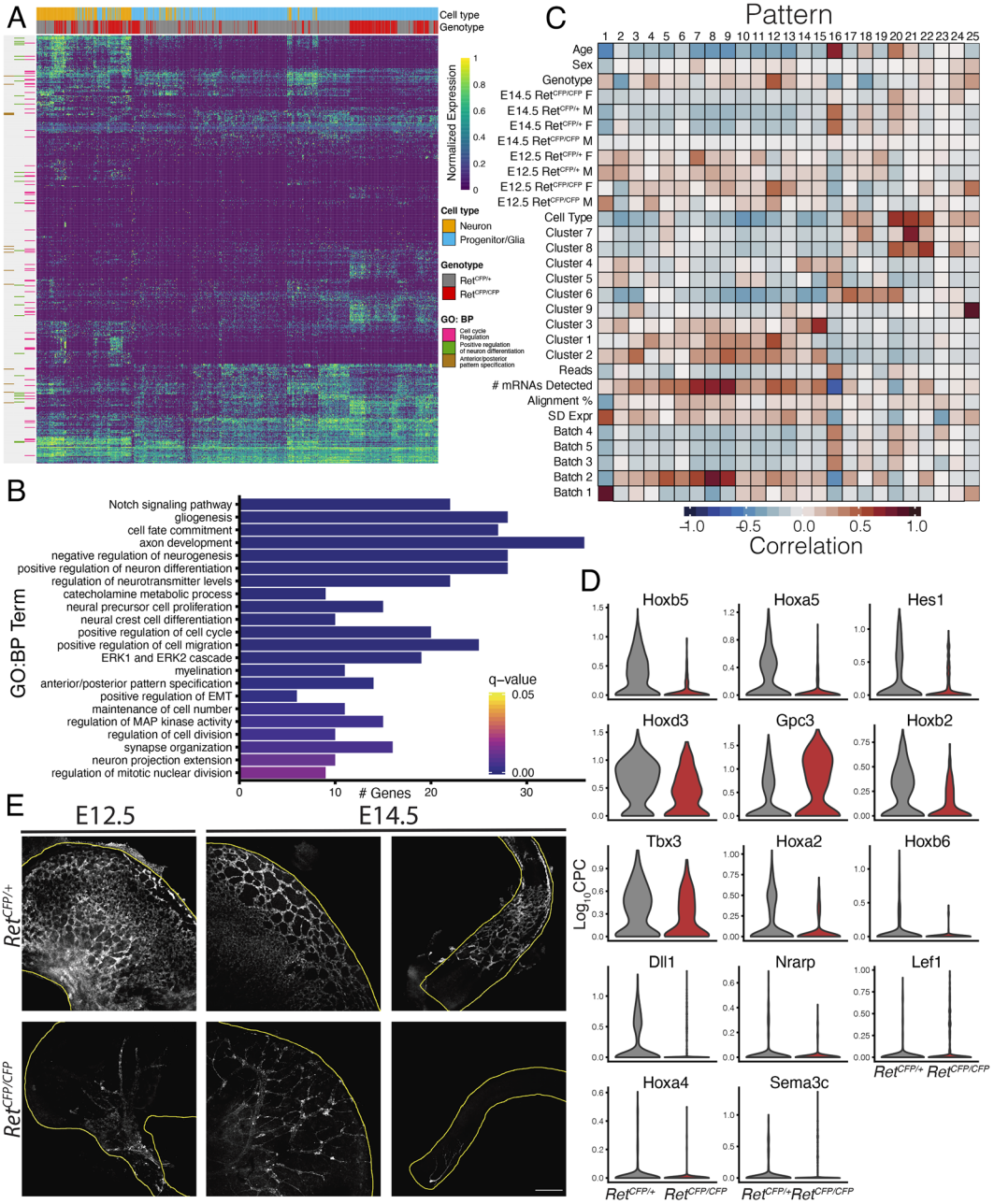

Fig. 2. Cellular and molecular changes driven by *Ret* loss of function. (*A*) Heatmap of genes DE with respect to genotype. (*B*) GO gene sets enriched for DE genes with respect to genotype (hypergeometric test, $P < 0.05$). (*C*) Correlation of scCoGAPS patterns with annotated cellular features. (*D*) Violin plots of DE genes associated with the anterior-posterior patterning GO term. (*E*) Immunofluorescence staining of mouse GI tract at E12.5 and E14.5 showing organization of CFP-expressing cells. Columns one and two show the stomach, and column three shows the hindgut. All IF images 10× magnification. (Scale bar, 200 μm.)

based on the expression of these 520 genes revealed that cells cluster first by cell type and then by genotype, again suggesting that the transcriptional changes observed are largely cell type specific. Gene ontology (GO) analysis revealed enrichment for several relevant processes, including gliogenesis, cell fate commitment, and axon development (hypergeometric test q value < 0.05, Fig. 2*B* and Dataset S7A). Significantly up-regulated genes expressed in $Ret^{CFP/CFP}$ progenitor/glia include several associated with glial maturation (*Fabp7*, *Plp1*, and *Myl9*) (44, 57), indicating that these progenitor/glia cells may be more mature than their $Ret^{CFP/+}$ counterparts. A second cluster of genes is more highly expressed in $Ret^{CFP/+}$ neurons and includes genes with specific expression in the neurogenic branch A (*Cartpt, Vip, Nos1,* and *Etv1*), consistent with our observation that $Ret^{CFP/+}$ cells are significantly overrepresented in branch A (cluster 7).

We next sought to map the transcriptional signatures learned from our ENCDC dataset to specific cellular features by using coordinated sets of coregulated genes. To this end, we applied scCoGAPS to learn 25 patterns of gene coexpression (*SI Appendix*, Fig. S6 and Dataset S8). We calculated the Pearson correlation for pattern weights by cell against both known and learned cellular annotations (Fig. 2*C* and Dataset S9). This revealed patterns that correlated with technical (read depth and alignment rates), experimental (genotype, age, and sex), as well as biological (cell type and cluster) variables. We identified patterns correlated with the acquisition of different neuronal identities (pattern 20: *Elavl4* (*HuD*), *Nrxn3, Tubb3, Nnat, Syt1*; pattern 21: *Nos1, Tubb2a, Mapt, Sncg,* and *Ntng1*; pattern 22: *Onecut2, Gabrg2, Gabra3, Slc18a3* (*VAChT*), *Gfra2, Elavl2,* and *Elavl3*) (*SI Appendix*, Fig. S6 and Dataset S10) (41), a transient neurogenic window (pattern 19: *Pou4f1, Gadd45g, Neurod4, Hes6, Btg1/2, Sox11,* and *Phox2b*) (24, 39), as well as glial identity (pattern 12: *S100b, Plp1,* and *Fabp7*) (24, 44, 57). We also identified patterns well correlated with specific genotype-biased clusters of cells including pattern 18 (*Ret, Gal, Ass1,* and *Etv1*) and pattern 21, specifically used by branch A neurons in cluster 7, and pattern 12, specifically used by cells in cluster 1 undergoing glial maturation and significantly enriched for $Ret^{CFP/CFP}$ cells.

Previous studies in mice have shown a severe migratory delay beginning as early as E9.5 in the absence of *Ret* (8, 17, 31). Consistent with this, we identified four gene expression patterns (patterns 2, 18, 19, and 25), well correlated with genotype, for which *Hox* family members were identified as pattern markers (58) (Dataset S10). Pattern 25 markers include the more distally expressed *Hoxa/c9* and *Hoxa/c10*. The separation of cluster 9 from the main manifold of ENCDCs, combined with the specific expression of marker genes such as *Maob* and *Pcdh10* (59–61), and specific usage of pattern 25, suggests that these cells are likely caudal SCPs. Enrichment for Hox genes within the remaining three pattern marker lists with strong correlation to genotype, suggests that Hox gene expression in ENCDCs may be a discriminating feature between the two genotypes. This was confirmed by the identification of seven *Hox* genes, (*Hoxa2*, *b2*, *d3*, and the more caudally expressed *Hoxa4*, *a5*, *b5*, and *b6*), as well as several anterior-posterior pattern specification genes (*Dll1, Gpc3, Hes1, Lef1, Nrarp, Sema3c,* and *Tbx3*), significantly DE (monocle likelihood ratio test; q < 0.05) with respect to genotype (Fig. 2 *A* and *B*). With the exception of *Gpc3, Lef1,* and *Sema3c*, all of the DE genes associated with anterior-posterior positioning show increased expression in $Ret^{CFP/+}$ cells (Fig. 2*D*). Consistent with this and other previous work at E12.5 (62), we observe that ENCDCs in the absence of *Ret* have not left the extrinsically innervating nerve fibers of the stomach by E12.5 nor by E14.5 (Fig. 2*E*), in stark contrast to $Ret^{CFP/+}$ cells which have formed a dense network throughout the stomach and all but the end of the hindgut by E12.5, as observed in the *Ret* heterozygous mouse model (31). As the *Hox* gene family is known to contribute to axial patterning, this differential expression of *Hox* genes may therefore be a consequence of significant rostrocaudal positional differences in ENCDCs in the presence and absence of *Ret*.

***Ret* Is Required for *Commitment* to the *B*ranch A Neuronal Developmental Trajectory.** Recent work in E15.5 mouse gut shows that after neuronal commitment cells of the developing ENS branch into two main trajectories, referred to here as branch A (*Etv1+, Gal+, Nos1+*, and *Vip+*) and branch B (*Bnc2+*, *Dlx5+*, *Mgat4c+*, and *Ndufa4l2+*) (14). Our UMAP embedding reveals this branching behavior can be observed as early as E12.5 and that the choice of branch is *Ret*-dependent (Fig. 3*A* and *SI Appendix*, Fig. S7*A*). As observed above, cluster 7 (branch A), is almost exclusively $Ret^{CFP/+}$ cells. Conversely, while cluster 8 (branch B) is significantly enriched for $Ret^{CFP/CFP}$ cells (Fig. 1*D*), both genotypes are represented along the branch B trajectory. This suggests a significant bias in the choice of developmental trajectory mediated in part by *Ret* expression in ENCDCs.

We next sought to identify branch-specific differences in gene expression with respect to genotype. When we tested cluster 8 (branch B), we identified 12 genes DE with respect to genotype (monocle likelihood ratio test, q < 0.05, Fig. 3*B* and Dataset S6B), four of which are more highly expressed in $Ret^{CFP/+}$ and eight more highly expressed in $Ret^{CFP/CFP}$. GO analysis indicates that genes up-regulated in $Ret^{CFP/CFP}$ are enriched (hypergeometric test, q < 0.05, Dataset S7B) for dopamine biosynthetic processes ($q < 4.52 \times 10^{-6}$, *Agtr2*, *Ddc*, and *Th*), catecholamine biosynthetic processes ($q < 6.44 \times 10^{-6}$, *Agtr2*, *Ddc*, and *Th*), and regulation of corticosteroid hormone secretion ($q < 3.35 \times 10^{-4}$, *Agtr2* and *Tac1*). This suggests that while both genotypes exhibit largely similar transcriptional profiles within branch B, we cannot rule out functional consequences of *Ret* LoF within this trajectory.

To examine differences between branch A and B trajectories and identify branch-specific markers, we tested for differential expression irrespective of genotype and identified 111 genes (monocle likelihood ratio test, q < 0.05, Fig. 3*C* and Dataset S6C). GO enrichment analysis (Dataset S7C) revealed that genes with higher expression in cluster 7 are enriched for regulation of neurological system processes (hypergeometric test, $q = 1.91 \times 10^{-5}$, *Cartpt, Ednrb, Fgfr1, Nos1, Nrg1,* and *Vip*) and axonogenesis ($q = 6.11 \times 10^{-5}$, *Ablim1, Auts2, Cdh11, Etv1, Lrrc4c, Lrrn3, Nrg1, Ntng1,* and *Ret*), while genes more highly expressed in cluster 8 are enriched for catecholamine biosynthetic processes ($q = 1.15 \times 10^{-8}$, *Agtr2, Dbh, Ddc, Gata3, Gch1,* and *Th*), regulation of neurotransmitter levels ($q = 2.00 \times 10^{-6}$, *Chrna7, Dbh, Ddc, Gch1, Nrxn1, Prima1, Slc18a1, Sytl4,* and *Th*), and dopamine biosynthetic processes ($q = 2.36 \times 10^{-6}$, *Agtr2, Dbh, Ddc, Gch1,* and *Th*). The increased expression of dopamine biosynthetic process genes in $Ret^{CFP/CFP}$ cells compared to $Ret^{CFP/+}$ cells within cluster 8 (Fig. 3*B*) suggests that differentiation and/or maturation rate of cells in branch B may be affected by loss of *Ret*. Additionally, several established markers of branches A and B (14) are DE in accordance with expectations: *Etv1, Gal, Nos1,* and *Vip* are higher in cluster 7/branch A; *Bnc2, Dlx5,* and *Ndufa4l2* are higher in cluster 8/branch B.

Both *Ret* and CFP are down-regulated in branch B, in addition to *Gfra1* (Fig. 3*D*), which encodes the canonical RET coreceptor, and *Ednrb*, which is epistatic with *Ret* (63–65). Interestingly, expression of these same genes is maintained in $Ret^{CFP/+}$ cells in branch A, and each exhibits a biased expression for cells along this trajectory (Fig. 3*D*). The exclusion of $Ret^{CFP/CFP}$ cells and persistent expression of *Ret* and *Gfra1* indicates that commitment to the branch A developmental trajectory, and subsequent establishment of the enteric neuronal subtypes derived from cells adopting this trajectory, requires continued *Ret* expression. The downregulation of both *Ret* and CFP expression in branch B, which contains numerous cells of both genotypes (Fig. 3 *A* and *D*), suggests that this trajectory does not require persistent *Ret* expression. While prior immunohistochemical studies found RET protein levels decrease in emerging glia and are maintained in emerging neurons (45), our scRNA-Seq data indicate that *Ret* expression is only maintained in the branch A neuronal trajectory and is down-regulated in the branch B trajectory, consistent with other recent single-cell studies (14, 16). Together these results suggest that a greater proportion of neuronally committed ENCDCs may engage the branch B trajectory in the absence of *Ret*, as branch A is an inaccessible developmental trajectory.

To validate branch A inaccessibility in $Ret^{CFP/CFP}$ ENCDCs, we selected the DE genes *Cartpt* (branch A/cluster 7) and *Gfra2* (branch B/cluster 8) as markers for in vivo validations due to their high expression and high specificity in each branch (Fig. 3*D*). We performed whole-mount immunohistochemistry (IHC) on the isolated gut (esophagus, stomach, and intestine) of $Ret^{CFP/+}$ and $Ret^{CFP/CFP}$ embryos at E12.5 and E14.5, to identify and localize cells from each branch. We probed for CART (encoded by *Cartpt*) and CFP to localize branch A cells. In $Ret^{CFP/+}$ samples at E12.5, we observe coexpression of CART and CFP in the stomach (Fig. 3*E*) but not in the esophagus. By E14.5, we observe coexpression of CART and CFP through to the hindgut of $Ret^{CFP/+}$ samples (Fig. 3*F*). Consistent with our scRNA-seq data, we do not observe CART expression in the stomach of $Ret^{CFP/CFP}$ samples at either age (Fig. 3 *E* and *F*), nor in the esophagus. We further validated the absence of branch A cells in $Ret^{CFP/CFP}$ intestine using single-molecule fluorescent in situ hybridization (RNAscope) to assess mRNA expression of the branch A marker genes *Cartpt* and *Gal* (*SI Appendix*, Fig. S7 *B* and *C*). These results demonstrate that cells associated with the branch A developmental trajectory are not produced within the GI tract in the absence of *Ret*.

To determine the spatial distribution of branch B cells, we assayed expression of *Gfra2*, which encodes a noncanonical RET

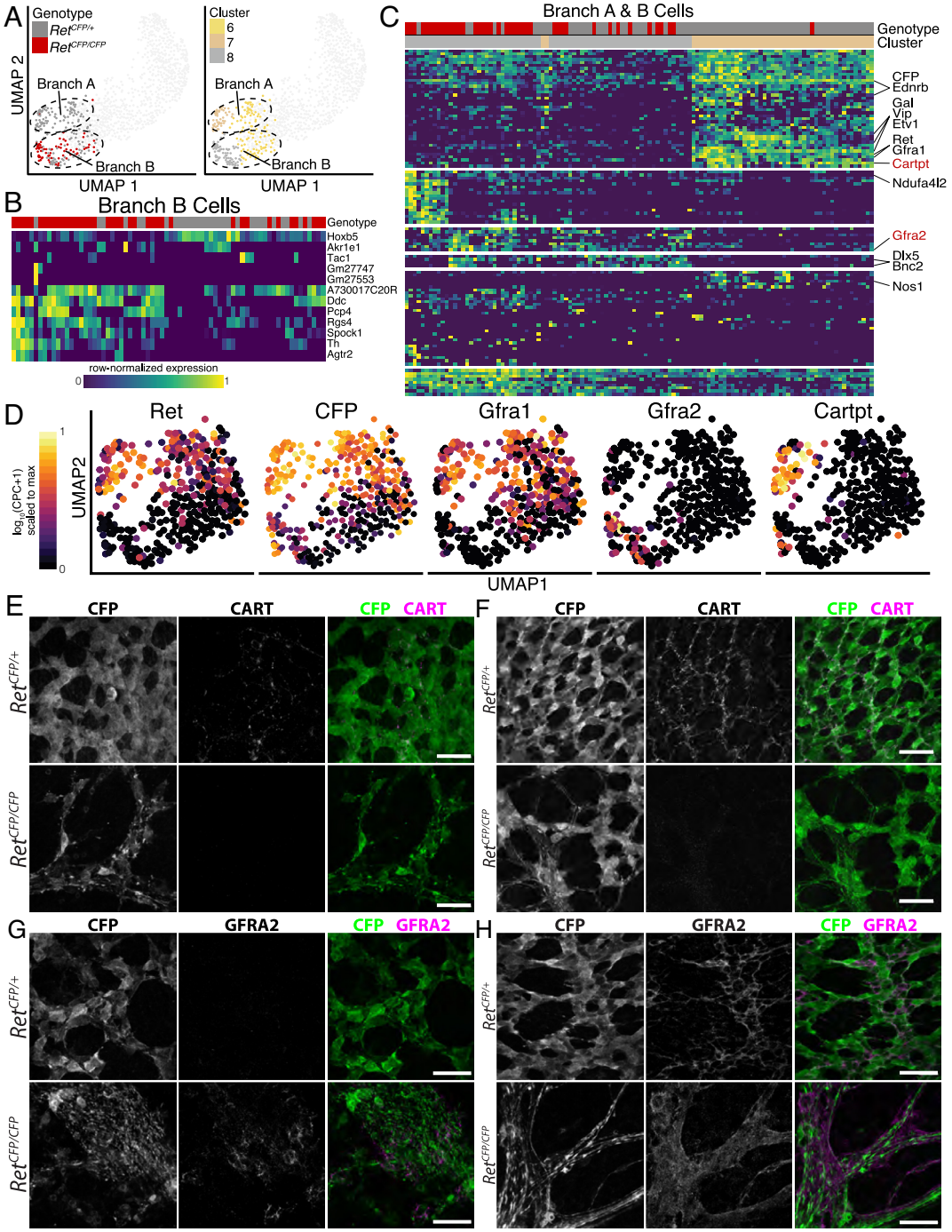

Fig. 3. *Ret* expression is required for access to the branch A developmental trajectory. (*A*) UMAP of neuronal cells comprising branches A and B colored by genotype (*Top*) and cluster (*Bottom*). (*B*) Heatmap of significantly DE genes with respect to genotype for branch B (cluster 8). (*C*) Heatmap of significantly DE genes between clusters 7 and 8, irrespective of genotype. Row cluster segmentation represents the top six divisions of the hierarchical clustering of gene expression values. (*D*) UMAPs demonstrating persistent expression of *Ret*, *CFP*, and *Gfra1* along the branch A developmental trajectory, induction of the noncanonical Ret coreceptor *Gfra2* in branch B, and branch A marker gene *Cartpt*. (*E* and *F*) Immunofluorescence assay of CART at (*E*) E12.5 in $Ret^{CFP/+}$ and $Ret^{CFP/CFP}$ stomach and (*F*) E14.5 in $Ret^{CFP/+}$ hindgut and $Ret^{CFP/CFP}$ stomach. (*G* and *H*) Immunofluorescence assay of GFRA2 at (*G*) E12.5 in $Ret^{CFP/+}$ and $Ret^{CFP/CFP}$ stomach and (*H*) E14.5 in $Ret^{CFP/+}$ hindgut and $Ret^{CFP/CFP}$ stomach. All IF images 60× magnification. (Scale bars, 40 μm.)

coreceptor and shows high, specific expression in branch B neurons. When we probed for GFRA2 and CFP via IHC, we did not observe GFRA2 expression in E12.5 $Ret^{CFP/+}$ stomach (Fig. 3*G*). We did, however, observe coexpression of GFRA2 and CFP restricted to cells along the extrinsically innervating nerve fibers of E12.5 $Ret^{CFP/CFP}$ stomach (Fig. 3*G*), confirming that branch B neuronal development trajectory is indeed accessible in the absence of *Ret*. At E12.5, we did not observe GFRA2 outside the extrinsically innervating nerve fibers of the $Ret^{CFP/CFP}$ stomach, nor in the intestines of either genotype, consistent with the previously described migratory defect and failure to effectively colonize the ENS in $Ret^{CFP/CFP}$ mice. We were able to detect putative branch B cells (CFP^+;$GFRA2^+$) in the esophagus in both genotypes, as well as non-neuronal ENCDCs (CFP^+;$GFRA2^-$) and maturing branch B cells (CFP^-;$GFRA2^+$) (*SI Appendix*, Fig. S7*D*), indicating that branch B cells are spatially restricted to the esophagus in E12.5 $Ret^{CFP/+}$ samples and to the esophagus and extrinsic nerve fibers along the stomach in E12.5 $Ret^{CFP/CFP}$. By E14.5, CFP^+/$GFRA2^+$ branch B maturing neurons are observed throughout the $Ret^{CFP/+}$ intestine; however, CFP^+/$GFRA2^+$ cells remain restricted to the extrinsically innervating nerve fibers along the stomach in $Ret^{CFP/CFP}$ embryos (Fig. 3*H*). Consistent with this difference, at E12.5 we see proportionally more $Ret^{CFP/CFP}$ cells in cluster 8 (branch B) than $Ret^{CFP/+}$ within our scRNA-Seq dataset (28/37 $Ret^{CFP/CFP}$) (Fig. 1*D*). By E14.5, however, $Ret^{CFP/+}$ are the predominant cells in cluster 8 (21/33 $Ret^{CFP/+}$) (Fig. 1*D*). This could be related to an overall reduced number of E14.5 $Ret^{CFP/CFP}$ cells in the intestine, or reduced capture efficiency as fluorescence decreases over biological time along this trajectory due to the downregulation of *Ret*, and by proxy CFP, as cells progress along branch B (Fig. 3*D*).

These data indicate that branch A and branch B represent two transcriptionally distinct developmental trajectories of maturing ENS neuronal subtypes that colonize the length of the intestines in the $Ret^{CFP/+}$ mice. Branch A neurons are never produced in $Ret^{CFP/CFP}$ embryos. Furthermore, branch B neurons are produced at a potentially faster developmental rate, but remain restricted to the extrinsically innervating nerve fibers throughout development in $Ret^{CFP/CFP}$ embryos. As *Ret* is required for cells to migrate into the developing ENS (Fig. 2*E*) (62) it follows that branch A, which appears to require *Ret*, would be inaccessible while branch B, which is *Ret*-independent, remains accessible in the absence of *Ret*.

HSCR-Associated Genes Are Expressed across Different Cellular States in the Developing ENS. While coding and enhancer LoF variants in *RET* contribute to ~50% of cases of HSCR, rare pathogenic alleles (PAs) in 23 additional genes are also associated with HSCR (19–22). Many of these genes are in the *RET-EDNRB* GRN that controls ENS development (20). To assess the profiles of HSCR-associated and *RET-EDNRB* GRN genes in our data, we investigated the expression pattern of 28 genes to determine their coexpression patterns and specific effects due to *Ret* LoF (Fig. 4*A*). Three HSCR-associated genes (*Gdnf, Edn3,* and *Nrtn*) are not expressed in our ENCDC dataset, as they are predominantly expressed by the surrounding gut mesenchyme. Of the remaining 21 expressed genes (*SI Appendix*, Fig. S8 *A–C*), six are significantly DE (monocle likelihood ratio test, q < 0.1, Fig. 4 *B* and *C* and Dataset S6A) between $Ret^{CFP/+}$ and $Ret^{CFP/CFP}$ cells (*Gfra1, Nrg1, Phox2b, Ednrb, Sema3c*, and *Sox10)*. To identify cell type–specific effects of *Ret* LoF, we next tested the combinatorial effect of genotype and cell type. Three HSCR-associated genes (*Gfra1, Sema3d,* and *Ednrb*) exhibit significant cell type–specific differential expression (monocle likelihood ratio test, q < 0.05, Fig. 4 *B* and *C* and Dataset S6D). *Gfra1* and *Ednrb* are significantly DE in both tests, suggesting a cell-autonomous effect of *Ret* LoF on the expression of these two genes. Conversely, four HSCR-associated genes (*Nrg1, Phox2b, Sema3c*, and *Sox10*) are globally DE but are not DE with respect to genotype:cell type interactions (monocle likelihood ratio test, q < 0.05; Dataset S6 A and D).

In addition to deviations in genotype proportion by cluster (Fig. 1*D*), we also observe that genotype proportions deviate significantly from expectation in E14.5 neurons and approach statistical significance in E14.5 glia (chi-squared test for equal proportions; neurons/P = 0.0158, glia/P = 0.0702) (Fig. 4*D*). Several HSCR-associated genes (*Ednrb, Gfra1, Elp1, Sox10,* and *Zeb2*) are expressed predominantly in progenitor/glia cells (*SI Appendix*, Fig. S8 *A* and *C*). *Phox2b, Tcf4,* and *Ubr4* are ubiquitously expressed across all clusters in our embedding (*SI Appendix*, Fig. S8 *A* and *C*). *L1cam* is enriched in both maturing neurons and maturing glia, but exhibits reduced expression within the cycling progenitor population (*SI Appendix*, Fig. S8 *A* and *C*), while *Ece1* appears predominantly expressed in maturing glial cells. These results suggest that global differential expression of HSCR-associated genes may in some cases be due to the confounding effects of differences in cell type proportions across genotypes. Finally, similar to the observed persistence of *Ret* expression along branch A, a subset of HSCR-associated genes are DE (monocle likelihood ratio test; q < 0.05, Dataset S6C) between the branches, with higher expression in branch A relative to branch B (*Ednrb, Gfra1, Nrg1*, and *Ret*), suggesting a potential role in the establishment of branch A identity in conjunction with *Ret*.

Despite significant genetic heterogeneity, ~67% of HSCR patients have mutations in *RET-EDNRB* GRN genes (19). The GRN includes bidirectional transcriptional feedback between *RET and EDNRB,* and the transcription factors *SOX10, GATA2, RARB,* and *NKX2-5*, as well as *GFRA1* and its ligand, *GDNF*, and the ubiquitin ligase *CBL*, which breaks down phosphorylated RET (20, 25, 64). To ascertain whether this feedback is cell-autonomous or nonautonomous, we examined

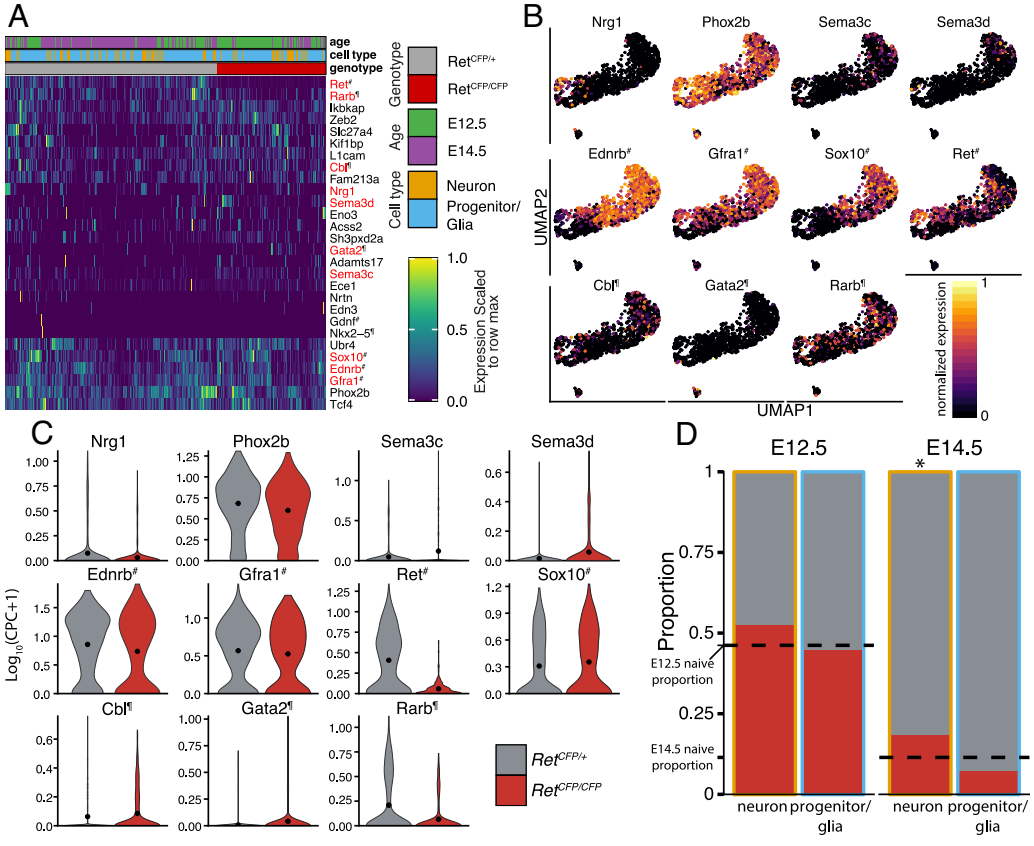

Fig. 4. Cellular diversity of Hirschsprung disease genes. (*A*) Heatmap 28 HSCR-associated and *RET-EDNRB* GRN genes across all cells. Significantly DE genes are highlighted in red. (*B*) UMAPs showing expression of 11 genes associated with HSCR and/or in the *RET-EDNRB* GRN, and DE with respect to genotype and/or genotype-cell type interactions (monocle likelihood ratio test q < 0.05). (*A* and *B*) # indicates genes both associated with HSCR and in the *RET-EDNRB* GRN, ¶ indicates genes in the *RET-EDNRB* GRN not previously associated with HSCR, and no notation indicates HSCR-associated genes not in the *RET-EDNRB* GRN. (*C*) Violin plots of these 11 genes show expression with respect to genotype, with mean expression value indicated by a dot. (*D*) Bar plot showing the proportion of neurons and progenitors/glia by genotype at E12.5 and E14.5. Dashed lines indicate the naive genotype proportion at E12.5 and E14.5. The asterisk indicates a significant deviance from the naive proportion (chi-squared test for equal proportions, P < 0.05).

the expression of these genes in our dataset. *Nkx2-5* and *Gdnf* are not expressed in our ENCDC dataset. Of the remaining six genes, four (*Gata2, Gfra1, Rarb,* and *Sox10*) are significantly DE between $Ret^{CFP/+}$ and $Ret^{CFP/CFP}$ ENCDCs (Dataset S6A), with *Gfra1* and *Rarb* more highly expressed in $Ret^{CFP/+}$ cells and *Sox10* and *Gata2* more highly expressed in $Ret^{CFP/CFP}$ cells, although these moderate differences in expression may also reflect a disproportionate distribution of ENS cell types within our dataset with respect to genotype (Fig. 4 *C* and *D* and *SI Appendix*, Fig. S8*C*). Finally, with the exception of *Sox10*, which rapidly decreases expression during neuronal commitment, and *Gata2*, which is specific to cluster 9, *Ednrb, Rarb, Gfra1*, and *Cbl* all exhibit persistent expression along the branch A neuronal developmental trajectory (Fig. 4*B* and *SI Appendix*, Fig. S8*C*), consistent with a role for the *RET-EDNRB* GRN in establishing branch A identity. The expression of *Sox10* exclusively within the progenitor population explains a previous observation that *Sox10* haploinsufficiency only affects the maintenance of progenitor cells and not neurons (66). These results highlight the diverse cellular states in which HSCR-associated genes are expressed, suggesting that their roles in HSCR disease etiopathology may involve modulation of different aspects of ENCDC proliferation and development. Collectively, however, *RET-EDNRB* GRN genes are affected by *Ret* LoF and are persistently expressed along the branch A trajectory, which is inaccessible in the $Ret^{CFP/CFP}$ mouse.

***Ret* LoF Reduces the Number of Actively Proliferating ENCDCs in the Developing Gut.** Reduction in proliferation capacity and precocious differentiation as a result of LoF of other genes within the developing ENS have been proposed as significant drivers of colonic aganglionosis (67, 68). Given the previously established role for *RET* as a proto-oncogene (18, 69) and its association with increased proliferation in other contexts (70–72), we asked whether *Ret* LoF was associated with significant differences in the proliferation rate of ENCDC progenitors. Differential gene expression analysis with respect to both genotype and cell type identified 331 genes (monocle likelihood ratio test, q < 0.05; *SI Appendix*, Fig. S9*A* and Dataset S6D), consisting of several genes associated with the mitotic cell cycle (*Cdkn1c, Cdk1, Top2a, Ccnd1, Cenpk, Cenpe, Cenpf, Ccna2, Ccnb1,* and *Ccnb2*), DNA replication (*Pcna, Mcm3, Mcm5, Mcm6, Mcm10,* and *Gmnn*), and cell cycle regulation (*Rgcc, Mad2l1, Chek2,* and *Rad51ap1*). Gene set enrichment analysis (GSEA) identified several cell cycle-associated gene sets including mitotic cell cycle processes, cell division, DNA replication, and regulation of cell cycle as top-scoring GO Biological Processes (BP) (hypergeometric test, q < 0.05; Dataset S7D). To focus on cells that are potentially engaging the cell cycle, we next performed a differential gene expression analysis on the subset of ENCDCs identified as progenitors or glia within the contiguous manifold (i.e., excluding ENCDCs committed to a postmitotic neuronal fate and excluding cluster 9). We identified 364 genes with significantly DE with respect to genotype (monocle likelihood ratio test, q < 0.05; Fig. 5*A* and Dataset S6E), and again GSEA identified gene sets associated with cell cycle regulation in addition to gliogenesis, cell fate commitment, and neural crest cell differentiation (hypergeometric test, q < 0.05; Fig. 5*B* and Dataset S7E). Thus, both cell cycle occupancy and differentiation state, two processes that are intrinsically linked during developmental fate specification, are disrupted in the $Ret^{CFP/CFP}$ progenitor population relative to $Ret^{CFP/+}$.

We next asked whether we could identify any significant differences in cell cycle state assignments for ENCDCs in the absence of *Ret*. We used the tricycle package (73) to project the 1,003 single ENCDCs into the default reference cell cycle space provided (Fig. 5*C*). This analysis allows us to estimate the continuous position of each cell along the cell cycle (Θ) (Dataset S11), comparisons of which by genotype and age (Fig. 5*D*) suggest that at E12.5 there are minimal differences in cell cycle occupancy between genotypes (Kolmogorov–Smirnov test; *P*-value = 0.660), but by E14.5, there are consistently fewer $Ret^{CFP/CFP}$ cells engaging the cell cycle than $Ret^{CFP/+}$ (Kolmogorov–Smirnov test; P value = 8.28×10^{-3}).

To further assess whether $Ret^{CFP/CFP}$ ENCDCs exhibit differential cell cycle occupancy relative to $Ret^{CFP/+}$, we next sought to infer cell cycle stage annotations for cells in our dataset using a projection-based approach with an independent, biologically relevant data source. Using the scCoGAPS patterns previously learned from publicly available data, and on which we trained the RF classification model, we observed high usage of three patterns within a population of cycling glia. GO enrichment analysis of pattern markers revealed these patterns correspond to different proliferative phases of the cell cycle (hypergeometric test, q < 0.05, Dataset S4 A and B). Pattern 40 is associated with DNA replication, corresponding to S phase; pattern 41 is associated with cilium assembly, organization, and segregation, and attachment of spindle microtubules to kinetochores, corresponding to prophase or metaphase (early M phase); and pattern 42 is associated with chromatid segregation and nuclear division, corresponding to anaphase or telophase (late M phase). To predict the cell cycle stage for individual cells in our ENCDC data, we scaled projected pattern weights linearly for each pattern to [0, 1] and interpreted these values as cell cycle stage occupancy probabilities (*SI Appendix*, Fig. S9 *C* and *D*). We tested all six possible comparisons of the four interaction conditions of genotype and age per pattern for differences in probabilities using two-sample Kolmogorov–Smirnov tests on the empirical cumulative density functions (*SI Appendix*, Fig. S9*E*) and used the Bonferroni method for multiple testing correction. Across the three patterns, E14.5 cells have significantly lower proliferative cell cycle stage occupancy probabilities than E12.5 cells of the same genotype (S phase: $Ret^{CFP/+}$ Bonferroni-adjusted $P = 1.32 \times 10^{-15}$, $Ret^{CFP/CFP}$ $P = 2.00 \times 10^{-15}$; early M: $Ret^{CFP/+}$ $P = 1.32 \times 10^{-15}$, $Ret^{CFP/CFP}$ $P = 3.84 \times 10^{-13}$; late M: $Ret^{CFP/+}$ $P = 1.38 \times 10^{-8}$, $Ret^{CFP/CFP}$ $P = 1.94 \times 10^{-9}$), consistent with the expectation that as progenitor cells differentiate, the proportion of actively cycling cells will decrease over biological time. Again, cell cycle stage occupancy probabilities for ENCDCs did not differ significantly with respect to genotype at E12.5. By E14.5, however, occupancy scores for $Ret^{CFP/CFP}$ cells are significantly lower across all three patterns (S phase: Bonferroni-adjusted $P = 9.66 \times 10^{-5}$, early M: $P = 1.97 \times 10^{-4}$; late M: $P = 0.0193$), suggesting overall fewer cycling ENCDCs in the $Ret^{CFP/CFP}$. This may be due to an increased differentiation rate, and consequently decreased proliferation rate, in $Ret^{CFP/CFP}$ cells compared to $Ret^{CFP/+}$ cells between E12.5 and E14.5.

To validate this predicted decrease in cell cycle occupancy in $Ret^{CFP/CFP}$ ENCDCs, we next used IHC to assess the number of CFP^+ ENCDCs coexpressing the mitotic marker phosphohistone H3 (pH3) within the developing gut at E14.5 (Fig. 5*E*). We confirmed a significant overall reduction in the number of CFP^+ cells in the $Ret^{CFP/CFP}$ mouse model at E14.5 (Student's t test, $P < 1.0 \times 10^{-4}$) (*SI Appendix*, Fig. S9*G*), consistent with the reduced number of CFP^+ cells observed in our FACS-collected population (Fig. 1*A*) and previously published studies (31). We also identified a slight difference in the mean number of $pH3^+$ cells at E14.5 (Student's t test, $P < 0.05$), though modest enough to suggest that the overall number of mitotic cells within the developing gut remains unaffected (*SI Appendix*, Fig. S9*H*). This is consistent with a cell-autonomous effect of *Ret* on the cell cycle, as ENCDCs make up a small portion of all proliferating cells in the developing gut and would therefore not contribute significantly to the overall proliferative capacity of the gut as a whole. The overall number of double positive $pH3^+/CFP^+$ cells was significantly reduced in $Ret^{CFP/CFP}$ embryos (Fig. 5*F* and *SI Appendix*, Fig. S7*I*) (Student's t test, $P = 0.029$), and while not statistically significant, we observed a difference in the mean percentage of $pH3^+$ cells within the subset of CFP^+ ENCDCs in the $Ret^{CFP/CFP}$ ENS at E14.5 indicating that a smaller fraction of developing ENCDCs are actively

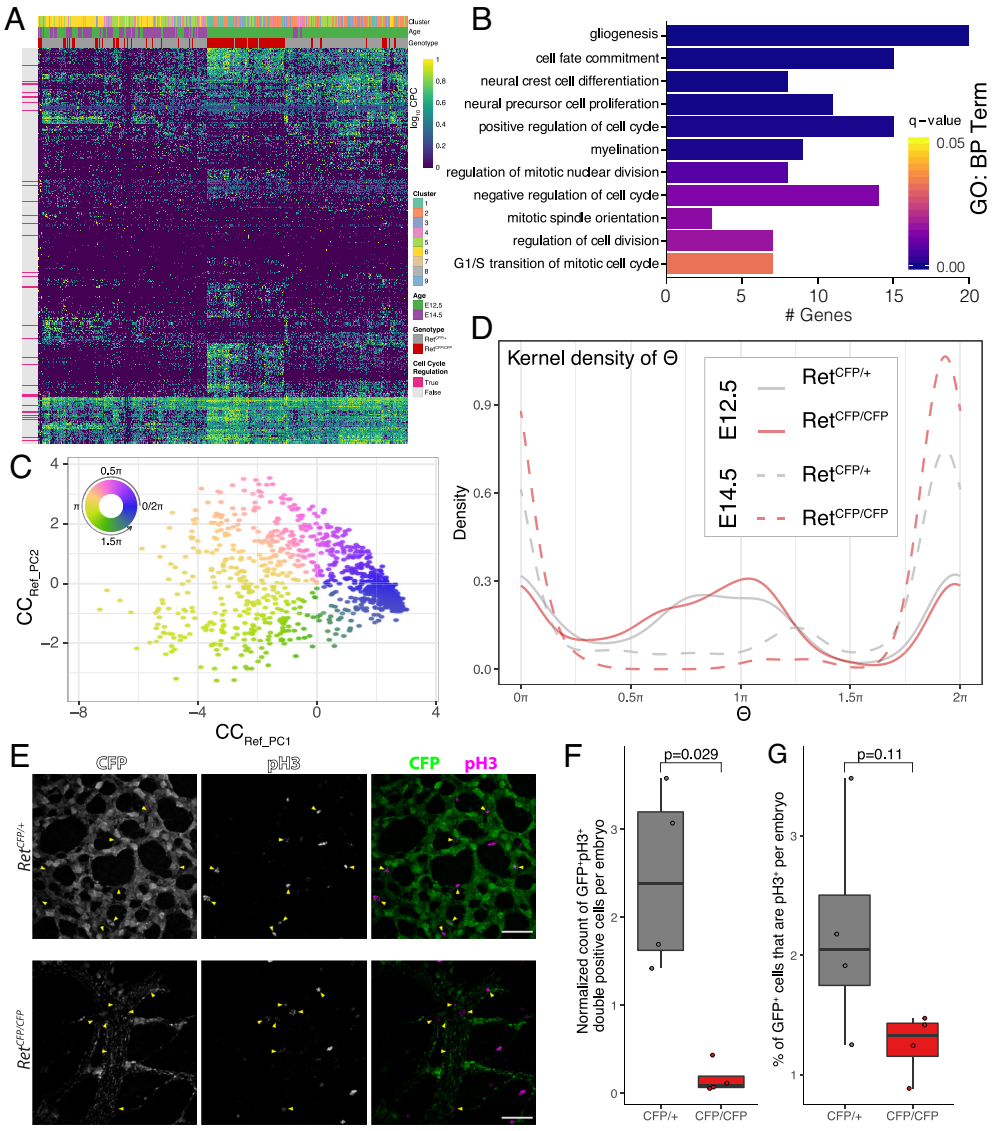

Fig. 5. Ret loss of function results in reduced cell cycle occupancy and a reduction in the number of actively proliferating ENCDC progenitors. (*A*) Heatmap of significantly DE genes with respect to genotype within the non-neuronal subset of ENCDCs. (*B*) Bar plots indicating the number of DE genes from (*A*) associated with each enriched GO:BP, along with *P* value for enrichment. (*C*) Tricycle embedding of ENCDCs to estimate cell cycle position. (*D*) Kernel density estimates for cell cycle position (θ) for each genotype at each age. Proliferative phase of the cell cycle (non-G0/G1) is between 0.25π and 1.75π. (*E*) Representative immunofluorescence staining of the proliferation marker pH3 and CFP in the stomach of E14.5 $Ret^{CFP/+}$ and $Ret^{CFP/CFP}$ mice. Yellow arrowheads indicate CFP^+ and $pH3^+$ double positive cells. All IF images 40× magnification. (Scale bars, 20 µm.) (*F*) Box and whiskers plot showing quantification of CFP^+ and $pH3^+$ double-positive cells per embryo, normalized by total microscope fields of view analyzed per embryo. (*G*) Box and whiskers plot showing the quantification of the % of CFP^+ cells with $pH3^+$ staining in the GI tract of E14.5 $Ret^{CFP/+}$ or $Ret^{CFP/CFP}$ mice.

engaging the cell cycle in the absence of *Ret* (Student's *t* test, $P = 0.11$) (Fig. 5*G* and *SI Appendix*, Fig. S9*J*). In aggregate, these results are consistent with the previously established role of *Ret* in enhancing proliferation and indicate that a loss of *Ret* in the developing ENS may contribute to an early reduction in the progenitor pool, possibly through induction of precocious differentiation, leading to a failure to colonize the more distal region of the developing gut.

Discussion

The ENS, initially derived entirely from the caudally migrating vagal and cranially migrating sacral neural crest cells, contains more than 100 million neurons of a variety of functionally distinct subtypes (74, 75). One of the critical genes that enables this transition of ENCDCs to diverse types of neurons is *RET,* the loss of function of which leads to HSCR. Despite the critical role *Ret* plays in ENS development, our understanding of the diversity of *Ret*-expressing cells in the developing GI tract, and the precise nature of the cell type–specific effects mediated by *Ret* LoF is limited. By performing scRNA-seq on enriched *Ret*-expressing cells during ENS development, we have generated a *Ret*-dependent fate transition map of ENCDCs to decipher the specific cellular phenotypes mediated by *Ret* LoF.

Our data indicate that the transcriptionally defined neuronal developmental state of ENCDCs bifurcates into excitatory and inhibitory motor neuron trajectories as early as E12.5, sooner than previously reported (14). Despite the understanding that ENCDCs may differentiate directly into neurons or via SCP (8), we observe no evidence to suggest that SCP- and non-SCP-derived neurons are transcriptionally distinct, either prior to or during this bifurcation. While our study captures major genetic and cellular changes due to *Ret* LoF at early developmental time points in the ENS, distinguishing transcriptional differences due to cell origin (e.g., SCP) versus *Ret* LoF exclusively would require lineage-tracing mouse models (8) at earlier time points. Furthermore, at this resolution, gross position within the developing gut does not appear to significantly alter the transcriptional state of branch B cells. While we observe branch B cells both in the intestines of $Ret^{+/CFP}$ animals and in the stomach of both genotypes, we do not observe position-dependent transcriptional signatures within branch B cells. Therefore, we propose that development of SCP-derived cells and non-SCP-derived cells follow the same general transcriptional program for ENC neuron differentiation.

***Ret* LoF Affects the Establishment of a Specific Developmental Neuronal Trajectory in the Developing GI Tract.** Our data demonstrate that *Ret*-expressing cells broadly acquire neuronal and glial fates early during development of the GI tract and help explain why *Ret* LoF leads to total aganglionosis caused by impaired migration,

defects in proliferation, and loss of immature ENCDCs (76). Our data highlight that *Ret* is required for the induction of an entire neuronal specification trajectory within the developing ENS which has previously been associated with the specific development of at least two distinct subtypes of inhibitory motor neurons: an interneuron subtype and a population of intrinsic primary afferent neurons (IPANs) (14). Although previous studies have posited that branch A corresponds to a predominantly inhibitory motor neuron (MN) trajectory and branch B corresponds to a predominantly excitatory MN trajectory (14), the developmental time points in our study prevent us from detecting this functional distinction given the lack of mature neurons.

Previous studies that characterized SCP-derived neurons in the adult gut as 80 to 90% excitatory cholinergic neurons defined this subclass based on the activity of the endogenous *Ret* promoter (8). Here, we have shown that the branch B developmental trajectory down-regulates Ret and CFP (Fig. 2*E*), indicating that the *Ret* promoter is likely deactivated during branch B cell maturation. While we are able to capture early branch B cells due to residual CFP, it is likely that residual CFP protein in branch B–derived cells will be undetectable by immunofluorescence by adolescence, when the proportion of primary excitatory neurons was described (8). Therefore, branch B cells would likely be specifically excluded from any study of the postnatal ENS that relies on the activity of the *Ret* promoter for detection. While the absence of branch A–derived cells may be the most relevant for HSCR disease etiology, the importance of the ability of branch B–derived cells to persist in the absence of RET should not be overlooked. At E12.5, we observe putative branch B cells ($GFRA2^+/CFP^+$) in the esophagus of the $Ret^{CFP/+}$ and in the esophagus and stomach of the $Ret^{CFP/CFP}$ mice (Fig. 3*F* and *SI Appendix*, Fig. S6*C*). We also observe branch A cells ($CART^+/CFP^+$) in the stomach of $Ret^{CFP/+}$ mice but not the esophagus, and we do not observe branch A cells anywhere in the $Ret^{CFP/CFP}$ GI tract at E12.5. By E14.5 we observe putative branch B cells in the stomach of the $Ret^{CFP/CFP}$, and throughout the gut in $Ret^{CFP/+}$ mice, consistent with published observations of both cell types in the small intestines of E15.5-E18.5 $Ret^{+/+}$ mice (14) The earlier establishment of branch B cells within the stomach of the $Ret^{CFP/CFP}$ is consistent with a model of precocious differentiation we identify in this study. The specific failure to produce cells along branch A in the $Ret^{CFP/CFP}$ suggests that the subset of mature ENS neuronal subtypes derived from this developmental trajectory may be the most acutely affected in disorders such as HSCR We provide evidence that aganglionosis observed in HSCR may arise from a combination of an early exit from the cell cycle for ENS progenitors, leading to precocious differentiation, and a failure to produce the full repertoire of mature ENS cell types. We do not detect any transcriptional signatures of cell death, suggesting that at this early time point, apoptosis or necrosis may not be a significant contributing factor in *Ret*-deficient aganglionosis. Our data suggest that *Ret* expression is not required for the establishment of a normal ENS glial identity; however, the observed effects on proliferation and differentiation potential suggest that enteric glia may be a preferred fate in *Ret* LoF models. Our data demonstrate that although the majority of *Ret* null cells in this particular model are associated with vagal nerve fibers in the proximal stomach, and likely vagal SCP-derived, a small proportion of these cells are actually located more caudally in the hindgut expressing markers of sacral SCP (*Th*+ and *Dbh*+). Since LoF variants in *RET* account for ~50% of HSCR patients (19), the presence of these cells in the hindgut (future colon) in a *Ret*-deficient background suggests that certain types of neurons might be still viable in these patients even in the aganglionic segments.

Neuronal Fates That Use Noncanonical *RET* Coreceptors Remain Accessible in the Absence of *Ret*. Compared to a previous study (14), we observe the divergence of the neuronal trajectories as early as E12.5, when ENCDCs are still migrating and undergoing neuronal maturation. While we observe a near complete absence of $Ret^{CFP/CFP}$ cells in branch A (cluster 7), we note that branch B (cluster 8) contains maturing neurons from both genotypes and is not grossly affected at the transcription level by loss of *Ret*. In the branch B trajectory, we observe a general reduction in the expression of *Ret*, *CFP*, and several *RET-EDNRB* GRN genes, including *Gfra1*, followed by upregulation of *Gfra2*, which encodes a noncanonical RET coreceptor. Although GFRA1 and GFRA2 are both in the GFRA family, GFRA1 preferentially binds GDNF as its ligand, while GFRA2 preferentially binds the GDNF family ligand NRTN. It is possible that GFRA2 binds to residual RET after downregulation of transcription; however, it raises the possibility that GFRA2 complexes with another coreceptor to activate an alternate signaling pathway responding to a different ligand in this *Ret*-independent trajectory. Differential expression of *Gfra* family genes within the aganglionic segment of HSCR patients has previously been observed (77), including a specific lack of *GFRA1* expression in neuronal cells within the associated hypertrophied nerve fibers. Additionally, *Ntrn* and *Gfra2* null mice exhibit a reduction in neuron fiber density and neuronal size in the ENS and in each case result in the specific loss of cholinergic excitatory myenteric innervation (presumably branch B derived) within the mouse gut, leaving the nitrergic neuronal population (branch A derived) largely unaffected (78, 79), consistent with the segregation of fates and corresponding gene expression differences described here. In aggregate, these results suggest that the canonical RET signaling pathway is responsible for the proper establishment of ENS subtypes derived from the branch A trajectory and that the activity of NRTN-GFRA2 signaling may play a greater role in the establishment of neuron identities along branch B, potentially independent from *Ret*.

Expression Patterns of HSCR-Associated Genes Highlight Necessity of Disease-Relevant Cellular Context. The specific expression patterns of many genes that harbor pathogenic alleles in HSCR patients within the ENCDCs of the ENS should lead us to reassess the nature of aganglionosis in HSCR. Our data highlight the need to better understand the specific cellular states and contexts in which these genes and GRNs operate, as well as the cell-autonomous versus cell nonautonomous effects in HSCR. Genes such as *Acss2, Eno2,* and *Adamts17* express very lowly in the ENS population (Fig. 4), yet are robustly expressed in both the mouse and human developing GI tract (19, 25). Furthermore, the design of our study allows us to only capture cell-autonomous effects; additional non-cell-autonomous effects have been observed in *Ret* LoF studies as well (80). Hence, patients carrying pathogenic alleles in the genes expressed in other cells may contribute to other GI anomalies, and aganglionosis may then be a secondary effect. Although verification of this would require detailed patient phenotyping, the shift between neuronal trajectories we have identified suggests developmental mechanisms that may guide future analysis of phenotypes.

***Ret* LoF Leads to Proliferation Defects in ENS Progenitors.** During formation of the ENS, the gut itself is increasing dramatically in both size and length, creating a huge proliferative burden on ENCDCs, the progenitors of the ENS. Our in silico estimates of cell cycle stage occupancy in conjunction with an in vivo assay of proliferation suggest a decrease in proliferation of ENCDCs in the absence of *Ret*. Even a small reduction in proliferative capacity could produce a significant decrease in population size over the course of the several days it takes to colonize the ENS, such as the absence of CFP+ cells we observe in the $Ret^{CFP/CFP}$ mouse intestines.

Ret deletion in the mouse leads to significant changes in fate acquisition, progenitor proliferation, and ENCDC migration within the developing ENS. It is likely that *RET* deficiency alleles in humans

lead to similar phenotypes in distinct subsets of ENS cell types and states in HSCR patients and that each of these phenotypes may play some combinatorial role in establishing the aganglionosis that is the hallmark of this disease. Furthermore, different *RET*-deficiency alleles and epistatic interactions may affect these phenotypes in different ways, potentially explaining some of the observed variable expressivity and incomplete penetrance of HSCR. Our study highlights the specific roles that *Ret* plays within different cellular contexts of the developing ENS and demonstrates that appropriate cellular context is critical for the interpretation of multiple disease-related cellular phenotypes that may emerge from a single causal insult.

Methods

Mouse Strains. *Ret CFP* knock-in mice ($Ret^{CFP/+}$; MGI:3777556) were generated by crossing $Ret^{fl/+}$ mice to β-actin-Cre mice to remove the *RET9* cDNA and maintained on a C57BL/6 background. All mouse experiments were conducted in accordance with the NIH Guidance for the Care and Use of Laboratory Animals. All procedures were approved by the Johns Hopkins Animal Care and Use Committee (Protocol number: MO21M56). All mice embryos used were either E12.5 or E14.5, and both male and female mice were used. Details of mouse breeding and genotyping are provided in *SI Appendix*.

Single-Cell RNA-Seq Library Preparation. Libraries were prepared from two embryos for each of the eight conditions ($Ret^{CFP/+}$ and $Ret^{CFP/CFP}$, female and male, E12.5 and E14.5) with two exceptions: libraries were prepared from 1 $Ret^{CFP/CFP}$ male E14.5 embryo and 4 $Ret^{CFP/CFP}$ female E14.5 embryos owing to differential viability. Single-cell RNA-seq libraries were prepared following a modified Smart-seq2 protocol (33, 34). Libraries were sequenced (paired end, 50 bp read length) on an Illumina HiSeq 2500 to an average depth of 9.91×10^5 (SD 7.43×10^5) paired-end reads per cell.

Data Preprocessing. Single-cell RNA-seq libraries were aligned with hisat2 version 2.0.1-beta to a mouse mm10 hisat2 index with the inserted CFP cDNA sequence included in the index. Using samtools 1.2, sam files were compressed to bam files and then sorted and indexed. Using Cufflinks v2.2.1 indexed bam files were quantified against the Gencode mouse vM10 assembly and normalized across all 1,369 samples (1,351 cells, 18 negative control wells). A total of 1,003 cells and 0 negative control wells passed quality control filters. The age, sex, and genotype of these 1,003 cells are as follows: 183 embryonic day (E)12.5 female $Ret^{CFP/+}$, 164 E12.5 male $Ret^{CFP/+}$, 173 E12.5 female $Ret^{CFP/CFP}$, 125 E12.5 male $Ret^{CFP/CFP}$, 161 E14.5 female $Ret^{CFP/+}$, 156 E14.5 male $Ret^{CFP/+}$, 37 E14.5 female $Ret^{CFP/CFP}$, and 4 E14.5 male $Ret^{CFP/CFP}$. FPKM values were transformed to CPC using the Census algorithm (37). Raw and processed data have been deposited in the NCBI Gene Expression Omnibus (GEO) under accession number GSE192676. Details of filtering constraints are provided in *SI Appendix*.

scRNA-Seq Analysis. To reduce the computational burden, analyses of gene expression were limited to expressed genes, defined as genes with nonzero CPC values in at least 20 cells and SD $>1 \times 10^{-20}$. Differential gene expression tests were performed using the Monocle R package (81). UMAP was performed on 419 high-dispersion genes using the Umapr R package (82, 83). RNAVelocity estimates were obtained using the Velocyto R package (49). Cluster assignment was performed using the mClust package (38). Specificity scores for each gene were calculated using the Jensen–Shannon (JS) distance from the cummeRbund package (84). Details of the selection of high-dispersion genes are provided in *SI Appendix*.

Seventy gene expression patterns were learned on 11,624 cells from publicly available scRNA-seq data from the ENS of adolescent mice (mousebrain.org) using scCoGAPS (47). We projected our data into these 70 patterns using projectR (47, 48). Twenty-five patterns were learned from our data, and we projected the publicly available data into these 25 patterns. Details of pattern discovery with scCoGAPS are provided in *SI Appendix*.

The random forest model was trained on all 1,105 neurons and a subset of 1,660 glia from the publicly available data described above (mousebrain.org) to create a 60:40 glia:neuron training dataset to avoid model bias. Glia were subsampled such that the distribution of glial cells across clusters in the subset matched the distribution across clusters in the whole glial population. The model was trained on 90% of cells to predict cluster assignment from 70 pattern weights with 10-fold cross-validation resulting in an accuracy of 89.8%. As pattern weights are constrained to [0,1], projected pattern weights were normalized to [0,1] before being used as input to predict cluster assignment. The parent cell type of each cluster was taken as the predicted cell type for our data.

Immunofluorescence Assay on the Whole Mouse Gut. Whole gut tissue (stomach, fore, and hindgut) at E12.5 and E14.5 was dissected and washed in ice-cold PBS followed by fixation in 4% PFA at 4 °C for 1 h. The fixed tissues were permeabilized and blocked in 5% normal donkey serum + 0.3% Triton-X for 1 h at room temperature (RT). The tissues were incubated with appropriate primary antibodies at 4 °C overnight, washed with PBS, and then incubated in appropriate secondary antibodies at 4 °C overnight (see Dataset S12 for antibodies and dilutions) followed by DAPI staining, mounting, and visualization. Details of immunofluorescence assays are provided in *SI Appendix*.

RNAscope. Fluorescence in situ hybridization was performed following the manufacturer's protocol for the RNAscope Fluorescent Multiplex V2 Assay using the RNAscope Multiplex Fluorescent Reagent Kit v2 (ACDBio #323100). Sections were deparaffinized and incubated in hydrogen peroxide for 10 m at RT and incubated in 1X Target Retrieval for 15 m at RT, then incubated in Protease Plus for 30 m at 40 °C. Sections were incubated in a 50:1:1 mixture of RNAscope Probes CFP (ACDBio #529381), Mm-Cartpt-C2 (ACDBio #432001-C2), and Mm-Gal-C3 (ACDBio #400961-C3) for 2 h at 40 °C. This was followed by standard steps per the manufacturer's instructions for staining and quenching. Sections were then incubated in RNAscope DAPI for 30 s at RT and mounted with ProLong Gold Antifade mounting media and imaged using a Nikon Eclipse Ti confocal microscope. A detailed protocol is provided in *SI Appendix*.

Proliferation Assay and Quantification. To measure cell cycle occupancy, we stained replicate $Ret^{CFP/+}$ and $Ret^{CFP/CFP}$ whole GI tracts from both male and female mice at E14.5 for phosphohistone H3 (Anti-H3S10p; Millipore Sigma #06-570), an immunomarker specific to cells undergoing mitosis (85), and CFP protein (Anti-GFP; Aves labs #GFP-1010) using the immunofluorescence assay described above. Confocal stack images were acquired on the Nikon Eclipse Ti confocal microscope with a 40× oil objective and type A immersion oil and quantified using a custom CellProfiler (86, 87) workflow. A detailed protocol is provided in *SI Appendix*.

Data, Materials, and Software Availability. Raw and processed sequencing reads data have been deposited in NCBI Gene Expression Omnibus (GEO) (GSE192676) (88).

ACKNOWLEDGMENTS. We would like to thank Hao Zhang at the JHU Cell Sorting facility for help with single-cell sorting. E.V. is supported in part by the Johns Hopkins Predoctoral Training Grant in Human Genetics (T32-GM007814-39). L.A.G. and E.V. are supported by an NIA R01 (R01AG066768). L.A.G. is additionally supported by the NIA (R01AG072305), the NSF (IOS-1665692), and a Johns Hopkins Catalyst award. S.C. is supported by an NYU Grossman School of Medicine Startup Grant (59-D-37802-30609-NYUPRJ), and A.C. is supported by an NICHD R01 award HD028088.

Author affiliations: [a]McKusick-Nathans Department of Genetic Medicine, Johns Hopkins University School of Medicine, Baltimore, MD 21205; [b]Center for Human Genetics and Genomics, New York University Grossman School of Medicine, New York, NY 10016; [c]Department of Neuroscience and Physiology, New York University Grossman School of Medicine, New York, NY 10016; [d]Solomon H. Snyder Department of Neuroscience, Johns Hopkins University School of Medicine, Baltimore, MD 21205; and [e]Kavli Neurodiscovery Institute, Johns Hopkins University, Baltimore, MD 21205

1. S. Kulkarni *et al.*, Neural crest-derived neurons are replaced by a newly identified mesodermal lineage in the post-natal and aging enteric nervous system. bioRxiv [Preprint] (2020). https://doi.org/10.1101/2020.08.25.262832 (Accessed 25 August 2020).
2. N. M. Le Douarin, J. Smith, Development of the peripheral nervous system from the neural crest. *Annu. Rev. Cell Biol.* **4**, 375–404 (1988).
3. S. Kulkarni *et al.*, Advances in enteric neurobiology: The "Brain" in the gut in health and disease. *J. Neurosci.* **38**, 9346–9354 (2018).
4. P. L. Durbec, L. B. Larsson-Blomberg, A. Schuchardt, F. Costantini, V. Pachnis, Common origin and developmental dependence on c-ret of subsets of enteric and sympathetic neuroblasts. *Development* **122**, 349–358 (1996).

5. R. P. Kapur, C. Yost, R. D. Palmiter, A transgenic model for studying development of the enteric nervous system in normal and aganglionic mice. *Development* **116**, 167–175 (1992).
6. H. M. Young *et al.*, A single rostrocaudal colonization of the rodent intestine by enteric neuron precursors is revealed by the expression of Phox2b, Ret, and p75 and by explants grown under the kidney capsule or in organ culture. *Dev. Biol.* **202**, 67–84 (1998).
7. A. M. Goldstein, R. M. W. Hofstra, A. J. Burns, Building a brain in the gut: Development of the enteric nervous system. *Clin. Genet.* **83**, 307–316 (2013).
8. T. Uesaka, M. Nagashimada, H. Enomoto, Neuronal differentiation in schwann cell lineage underlies postnatal neurogenesis in the enteric nervous system. *J. Neurosci.* **35**, 9879–9888 (2015).
9. J. B. Furness, The enteric nervous system and neurogastroenterology. *Nat. Rev. Gastroenterol. Hepatol.* **9**, 286–294 (2012).
10. R. O. Heuckeroth, Hirschsprung disease–Integrating basic science and clinical medicine to improve outcomes. *Nat. Rev. Gastroenterol. Hepatol.* **15**, 152–167 (2018).
11. M. M. Hao, H. M. Young, Development of enteric neuron diversity. *J. Cell. Mol. Med.* **13**, 1193–1210 (2009).
12. Y.-N. Kang, C. Fung, P. V. Berghe, Gut innervation and enteric nervous system development: A spatial, temporal and molecular tour de force. *Development* **148**, dev182543 (2021).
13. R. Lasrado *et al.*, Lineage-dependent spatial and functional organization of the mammalian enteric nervous system. *Science* **356**, 722–726 (2017).
14. K. Morarach *et al.*, Diversification of molecularly defined myenteric neuron classes revealed by single-cell RNA sequencing. *Nat. Neurosci.* **24**, 34–46 (2021).
15. K. Morarach *et al.*, Single-cell molecular interrogation of enteric nervous system development. *Mech. Dev.* **145**, S67 (2017).
16. R. Elmentaite *et al.*, Cells of the human intestinal tract mapped across space and time. *Nature* **597**, 250–255 (2021).
17. D. Natarajan, C. Marcos-Gutierrez, V. Pachnis, E. de Graaff, Requirement of signalling by receptor tyrosine kinase RET for the directed migration of enteric nervous system progenitor cells during mammalian embryogenesis. *Development* **129**, 5151–5160 (2002).
18. L. M. Mulligan, RET revisited: Expanding the oncogenic portfolio. *Nat. Rev. Cancer* **14**, 173–186 (2014).
19. J. M. Tilghman *et al.*, Molecular genetic anatomy and risk profile of Hirschsprung's disease. *N. Engl. J. Med.* **380**, 1421–1432 (2019).
20. S. Chatterjee *et al.*, Enhancer variants synergistically drive dysfunction of a gene regulatory network in Hirschsprung disease. *Cell* **167**, 355–368.e10 (2016).
21. A. Kapoor *et al.*, Population variation in total genetic risk of Hirschsprung disease from common RET, SEMA3 and NRG1 susceptibility polymorphisms. *Hum. Mol. Genet.* **24**, 2997–3003 (2015).
22. S. Chatterjee, K. M. Karasaki, L. E. Fries, A. Kapoor, A. Chakravarti, A multi-enhancer RET regulatory code is disrupted in Hirschsprung disease. *Genome Res.* **31**, 2199–2208 (2021).
23. M. M. Alves *et al.*, Contribution of rare and common variants determine complex diseases-Hirschsprung disease as a model. *Dev. Biol.* **382**, 320–329 (2013).
24. T. A. Heanue, V. Pachnis, Expression profiling the developing mammalian enteric nervous system identifies marker and candidate Hirschsprung disease genes. *Proc. Natl. Acad. Sci. U.S.A.* **103**, 6919–6924 (2006).
25. S. Chatterjee, P. Nandakumar, D. R. Auer, S. B. Gabriel, A. Chakravarti, Gene- and tissue-level interactions in normal gastrointestinal development and Hirschsprung disease. *Proc. Natl. Acad. Sci. U.S.A.* **116**, 26697–26708 (2019).
26. E. M. Southard-Smith, L. Kos, W. J. Pavan, Sox10 mutation disrupts neural crest development in Dom Hirschsprung mouse model. *Nat. Genet.* **18**, 60–64 (1998).
27. D. Lang *et al.*, Pax3 is required for enteric ganglia formation and functions with Sox10 to modulate expression of c-ret. *J. Clin. Invest.* **106**, 963–971 (2000).
28. A. Pattyn, X. Morin, H. Cremer, C. Goridis, J. F. Brunet, The homeobox gene Phox2b is essential for the development of autonomic neural crest derivatives. *Nature* **399**, 366–370 (1999).
29. N. Nagy, A. M. Goldstein, Enteric nervous system development: A crest cell's journey from neural tube to colon. *Semin. Cell Dev. Biol.* **66**, 94–106 (2017).
30. F. Obermayr, R. Hotta, H. Enomoto, H. M. Young, Development and developmental disorders of the enteric nervous system. *Nat. Rev. Gastroenterol. Hepatol.* **10**, 43–57 (2013).
31. T. Uesaka, M. Nagashimada, S. Yonemura, H. Enomoto, Diminished Ret expression compromises neuronal survival in the colon and causes intestinal aganglionosis in mice. *J. Clin. Invest.* **118**, 1890–1898 (2008).
32. A. Kapoor, D. R. Auer, D. Lee, S. Chatterjee, A. Chakravarti, Testing the Ret and Sema3d genetic interaction in mouse enteric nervous system development. *Hum. Mol. Genet.* **26**, 1811–1820 (2017).
33. S. Picelli *et al.*, Full-length RNA-seq from single cells using Smart-seq2. *Nat. Protoc.* **9**, 171–181 (2014).
34. M. Chevée, J. D. J. Robertson, G. H. Cannon, S. P. Brown, L. A. Goff, Variation in activity state, axonal projection, and position define the transcriptional identity of individual neocortical projection neurons. *Cell Rep.* **22**, 441–455 (2018).
35. J. Amiel *et al.*, Hirschsprung disease, associated syndromes and genetics: A review. *J. Med. Genet.* **45**, 1–14 (2008).
36. R. Dang *et al.*, Genetic background strongly modifies the severity of symptoms of Hirschsprung disease, but not hearing loss in rats carrying Ednrb^{sl} mutations. *PLoS One* **6**, e24086 (2011).
37. X. Qiu *et al.*, Single-cell mRNA quantification and differential analysis with Census. *Nat. Methods* **14**, 309–315 (2017).
38. L. Scrucca, M. Fop, T. B. Murphy, A. E. Raftery, mclust 5: Clustering, classification and density estimation using Gaussian finite mixture models. *R J.* **8**, 289–317 (2016).
39. S. Tutukova, V. Tarabykin, L. R. Hernandez-Miranda, The role of neurod genes in brain development, function, and disease. *Front. Mol. Neurosci.* **14**, 662774 (2021).
40. S. Jhas *et al.*, Hes6 inhibits astrocyte differentiation and promotes neurogenesis through different mechanisms. *J. Neurosci.* **26**, 11061–11071 (2006).
41. E. Drokhlyansky *et al.*, The human and mouse enteric nervous system at single-cell resolution. *Cell* **182**, 1606–1622.e23 (2020).
42. C. M. Wright *et al.*, scRNA-Seq reveals new enteric nervous system roles for GDNF, NRTN, and TBX3. *Cell Mol. Gastroenterol. Hepatol.* **11**, 1548–1592.e1 (2021).
43. F. Memic *et al.*, Transcription and signaling regulators in developing neuronal subtypes of mouse and human enteric nervous system. *Gastroenterology* **154**, 624–636 (2018).
44. M. Rao *et al.*, Enteric glia express proteolipid protein 1 and are a transcriptionally unique population of glia in the mammalian nervous system. *Glia* **63**, 2040–2057 (2015).
45. H. M. Young, D. Ciampoli, J. Hsuan, A. J. Canty, Expression of Ret-, p75(NTR)-, Phox2a-, Phox2b-, and tyrosine hydroxylase-immunoreactivity by undifferentiated neural crest-derived cells and different classes of enteric neurons in the embryonic mouse gut. *Dev. Dyn.* **216**, 137–152 (1999).
46. A. Zeisel *et al.*, Molecular architecture of the mouse nervous system. *Cell* **174**, 999–1014.e22 (2018).
47. G. L. Stein-O'Brien *et al.*, Decomposing cell identity for transfer learning across cellular measurements, platforms, tissues, and species. *Cell Syst.* **8**, 395–411.e8 (2019).
48. G. Sharma, C. Colantuoni, L. A. Goff, E. J. Fertig, G. Stein-O'Brien, projectR: An R/Bioconductor package for transfer learning via PCA, NMF, correlation, and clustering. *Bioinformatics* **36**, 3592–3593 (2019).
49. G. La Manno *et al.*, RNA velocity of single cells. *Nature* **560**, 494–498 (2018).
50. L. R. Borlado, J. Méndez, CDC6: From DNA replication to cell cycle checkpoints and oncogenesis. *Carcinogenesis* **29**, 237–243 (2008).
51. J. Pines, T. Hunter, Isolation of a human cyclin cDNA: Evidence for cyclin mRNA and protein regulation in the cell cycle and for interaction with p34cdc2. *Cell* **58**, 833–846 (1989).
52. C. S. Hirst *et al.*, Kif1bp loss in mice leads to defects in the peripheral and central nervous system and perinatal death. *Sci. Rep.* **7**, 16676 (2017).
53. I. Espinosa-Medina *et al.*, Dual origin of enteric neurons in vagal Schwann cell precursors and the sympathetic neural crest. *Proc. Natl. Acad. Sci. U.S.A.* **114**, 11980–11985 (2017).
54. A. J. Burns, N. M. Douarin, The sacral neural crest contributes neurons and glia to the post-umbilical gut: Spatiotemporal analysis of the development of the enteric nervous system. *Development* **125**, 4335–4347 (1998).
55. N. M. L. Douarin, M.-A. Teillet, The migration of neural crest cells to the wall of the digestive tract in avian embryo. *Development* **30**, 31–48 (1973).
56. R. P. Kapur, Colonization of the murine hindgut by sacral crest-derived neural precursors: Experimental support for an evolutionarily conserved model. *Dev. Biol.* **227**, 146–155 (2000).
57. H. M. Young, A. J. Bergner, T. Müller, Acquisition of neuronal and glial markers by neural crest-derived cells in the mouse intestine. *J. Comp. Neurol.* **456**, 1–11 (2003).
58. G. L. Stein-O'Brien *et al.*, PatternMarkers & GWCoGAPS for novel data-driven biomarkers via whole transcriptome NMF. *Bioinformatics* **33**, 1892–1894 (2017).
59. M. R. Sapio, S. C. Goswami, J. R. Gross, A. J. Mannes, M. J. Iadarola, Transcriptomic analyses of genes and tissues in inherited sensory neuropathies. *Exp. Neurol.* **283**, 375–395 (2016).
60. N. P. Gonçalves, D. Martins, M. J. Saraiva, Overexpression of protocadherin-10 in transthyretin-related familial amyloidotic polyneuropathy. *Am. J. Pathol.* **186**, 1913–1924 (2016).
61. A. M. Stevens, L. Liu, D. Bertovich, J. M. Janjic, J. A. Pollock, Differential Expression of Neuroinflammatory mRNAs in the Rat Sciatic Nerve Following Chronic Constriction Injury and Pain-Relieving Nanoemulsion NSAID Delivery to Infiltrating Macrophages. *Int. J. Mol. Sci.* **20**, 5269 (2019).
62. C. S. Hirst *et al.*, Publisher Correction: Kif1bp loss in mice leads to defects in the peripheral and central nervous system and perinatal death. *Sci. Rep.* **8**, 9085 (2018).
63. A. S. McCallion, E. Stames, R. A. Conlon, A. Chakravarti, Phenotype variation in two-locus mouse models of Hirschsprung disease: Tissue-specific interaction between Ret and Ednrb. *Proc. Natl. Acad. Sci. U.S.A.* **100**, 1826–1831 (2003).
64. S. Chatterjee, A. Chakravarti, A gene regulatory network explains RET-EDNRB epistasis in Hirschsprung disease. *Hum. Mol. Genet.* **28**, 3137–3147 (2019).
65. M. M. Carrasquillo *et al.*, Genome-wide association study and mouse model identify interaction between RET and EDNRB pathways in Hirschsprung disease. *Nat. Genet.* **32**, 237–244 (2002).
66. C. Paratore, C. Eichenberger, U. Suter, L. Sommer, Sox10 haploinsufficiency affects maintenance of progenitor cells in a mouse model of Hirschsprung disease. *Hum. Mol. Genet.* **11**, 3075–3085 (2002).
67. N. Fujiwara *et al.*, Altered expression of laminin alpha1 in aganglionic colon of endothelin receptor-B null mouse model of Hirschsprung's disease. *Pediatr. Surg. Int.* **34**, 137–141 (2018).
68. K.-F. Bergeron *et al.*, Upregulation of the Nr2f1-A830082K12Rik gene pair in murine neural crest cells results in a complex phenotype reminiscent of Waardenburg syndrome type 4. *Dis. Model. Mech.* **9**, 1283–1293 (2016).
69. M. Grieco *et al.*, PTC is a novel rearranged form of the ret proto-oncogene and is frequently detected in vivo in human thyroid papillary carcinomas. *Cell* **60**, 557–563 (1990).
70. H.-J. Park, E. C. Bolton, RET-mediated glial cell line-derived neurotrophic factor signaling inhibits mouse prostate development. *Development* **144**, 2282–2293 (2017).
71. D. Perea *et al.*, Ret receptor tyrosine kinase sustains proliferation and tissue maturation in intestinal epithelia. *EMBO J.* **36**, 3029–3045 (2017).
72. A. Gattelli *et al.*, Ret inhibition decreases growth and metastatic potential of estrogen receptor positive breast cancer cells. *EMBO Mol. Med.* **5**, 1335–1350 (2013).
73. S. Zheng *et al.*, Universal prediction of cell cycle position using transfer learning. *Genome Biol.* **23**, 41 (2022).
74. J. B. Furness, The enteric nervous system: Normal functions and enteric neuropathies. *Neurogastroenterol. Motil.* **20**, 32–38 (2008).
75. M. Rao, M. D. Gershon, The bowel and beyond: The enteric nervous system in neurological disorders. *Nat. Rev. Gastroenterol. Hepatol.* **13**, 517–528 (2016).
76. A. Schuchardt, V. D'Agati, L. Larsson-Blomberg, F. Costantini, V. Pachnis, Defects in the kidney and enteric nervous system of mice lacking the tyrosine kinase receptor Ret. *Nature* **367**, 380–383 (1994).
77. V. C. H. Lui, E. T. Samy, M. H. Sham, L. M. Mulligan, P. K. H. Tam, Glial cell line-derived neurotrophic factor family receptors are abnormally expressed in aganglionic bowel of a subpopulation of patients with Hirschsprung's disease. *Lab. Invest.* **82**, 703–712 (2002).
78. J. Rossi *et al.*, Retarded growth and deficits in the enteric and parasympathetic nervous system in mice lacking GFRα2, a functional neurturin receptor. *Neuron* **22**, 243–252 (1999).
79. R. O. Heuckeroth *et al.*, Gene targeting reveals a critical role for neurturin in the development and maintenance of enteric, sensory, and parasympathetic neurons. *Neuron* **22**, 253–263 (1999).
80. S. Bogni, P. Trainor, D. Natarajan, R. Krumlauf, V. Pachnis, Non-cell-autonomous effects of Ret deletion in early enteric neurogenesis. *Development* **135**, 3007–3011 (2008).
81. C. Trapnell *et al.*, The dynamics and regulators of cell fate decisions are revealed by pseudotemporal ordering of single cells. *Nat. Biotechnol.* **32**, 381–386 (2014).
82. L. McInnes, J. Healy, N. Saul, L. Großberger, UMAP: Uniform manifold approximation and projection. *J. Open Source Softw.* **3**, 861 (2018).
83. A. Li, J. Kim, M. Smith, S. Hughes, T. Laderas, *umapr: ARCHIVED UMAP dimensionality reduction in R* (rOpenSci Unconference 2018, Seattle, WA) https://github.com/ropensci-archive/umapr. Accessed 22 October 2021.
84. L. Goff, C. Trapnell, D. Kelley, cummeRbund: Analysis, Exploration, Manipulation, and Visualization of Cufflinks High-Throughput Sequencing Data (R Package Version 2, Bioconductor, 2013) https://rdrr.io/bioc/cummeRbund/.
85. I. Skaland, E. A. M. Janssen, E. Gudlaugsson, L. H. R. Guo, J. Baak, The prognostic value of the proliferation marker phosphohistone H3 (PPH3) in luminal, basal-like and triple negative phenotype invasive lymph node-negative breast cancer. *Anal. Cell. Pathol.* **31**, 261–271 (2009).
86. A. E. Carpenter *et al.*, Cell Profiler: Image analysis software for identifying and quantifying cell phenotypes. *Genome Biol.* **7**, R100 (2006).
87. C. McQuin *et al.*, Cell Profiler 3.0: Next-generation image processing for biology. *PLoS Biol.* **16**, e2005970 (2018).
88. E. Vincent *et al.*, Ret loss-of-function decreases neural crest progenitor proliferation and restricts developmental fate potential during enteric nervous system development. NCBI Gene Expression Omnibus. https://www.ncbi.nlm.nih.gov/geo/query/acc.cgi?acc=GSE192676. Accessed 30 December 2021.